Carbohydrate Polymers 86 (2011) 1699–1704

Contents lists available at ScienceDirect

Carbohydrate Polymers

journal homepage: www.elsevier.com/locate/carbpol

Fabrication and characterization of zirconium hydroxide-carboxymethyl cellulose sodium/plasticized *Trichosanthes Kirilowii* starch nanocomposites

Dan Liu[a], Peter R. Chang[b], Sha Deng[c], Chuangyuan Wang[c], Baojing Zhang[c], Yan Tian[c], Shanshan Huang[c], Jihong Yao[c], Xiaochi Ma[c,*]

[a] *School of Science, Dalian Nationalities University, Dalian 116600, China*
[b] *Bioproducts and Bioprocesses National Science Program, Agriculture and Agri-Food Canada, 107 Science Place, Saskatoon, SK, S7N 0X2, Canada*
[c] *School of Pharmaceutical Sciences, Dalian Medical University, Dalian 116044, China*

ARTICLE INFO

Article history:
Received 13 June 2011
Received in revised form 28 June 2011
Accepted 30 June 2011
Available online 7 July 2011

Keywords:
Zirconium hydroxide
Carboxymethylcellulose sodium (CMC)
Starch
Trichosanthes kirilowii

ABSTRACT

Carboxymethyl cellulose sodium (CMC) was used as the template to prepare zirconium hydroxide nanoparticles. The resulted Zr-CMC was composed of about 29.4 wt% CMC and amorphous zirconium hydroxide. Zirconium hydroxide nanoparticles in size of 20–50 nm were encapsulated by CMC, which could improve the stability of zirconium hydroxide in water. *Trichosanthes kirilowii* (*TK*) is a traditional Chinese medicine, which is rich in starch. *TK* starch is attempted to be plasticized with glycerol to obtain glycerol-plasticized starch (GPS) in the casting process. And Zr-CMC as the filler was loaded in GPS matrix. Since Zr-CMC could form the good interaction with GPS matrix, Zr-CMC filler could be dispersed well in GPS matrix; thereby, improve the mechanical properties and water barrier of GPS matrix.

Crown Copyright © 2011 Published by Elsevier Ltd. All rights reserved.

1. Introduction

Much effort has made to develop biodegradable materials because of the worldwide environment and resources problems resulted from petroleum-derived plastics. Starch is one of the most promising raw materials and commercially available ingredients for the production of biodegradable plastics because of a great variety of crop sources. Many crop starches have been used to prepare the plasticized starch (PS) such as corn (Mondragon, Mancilla, & Rodriguez-Gonzalez, 2008), wheat (Averous, Moro, Dole, & Fringant, 2000), barley, oat (Forssell, Hulleman, Myllärinen, Moates, & Parker, 1999), rice (Dias, Müller, Larotonda, & Laurindo, 2010), potato starch (Smits, Kruiskamp, van Soest, & Vliegenthart, 2003), cassava starch (Mali, Grossmann, García, Martino, & Zaritzky, 2006) and pea starch (Ma, Chang, Yang, & Yu, 2009). Some medicinal plants are also found to contain a large number of starches in the bulb or roots. Only active pharmaceutical ingredients are concerned on and extracted for the therapy, however, starch components are usually discarded. Recent researches have been carried out on the starch sourced from medicinal plants, in order to make good use of medicinal plant resources and widen their industrial application.

Starches from Bai-zhi (*Angelica dahurica*) (Zhou, Wang, Zhao, Fang, & Sun, 2010), Tian-hua-fen (*Trichosanthes kirilowii*), Ha-soo-Oh (*Polygonum multiflorum*) (Ma, Chang, Zheng, Yu, & Ma, 2010), Bei-mu (*Fritillaria*) (Wang et al., 2007) and yam (*Dioscorea opposita* Thunb) (Wang, Yu, Zhu, Yu, & Jin, 2009) have been investigated on the physicochemical properties. The yam starch has been plasticized to prepare PS (Xie, Chang, Wang, Yu, & Ma, 2011). In this work, *T. kirilowii* (Chinese name Tian-hua-fen) starch is attempted to be plasticized to prepare glycerol-plasticized starch (GPS) matrix in the casting process.

Compared to synthetic polymers, PS often exhibits poor mechanical properties and the relatively huge water uptake. The introduction of nanofillers can improve the mechanical properties and water resistance of GPS matrix, but the good interaction between the nanofillers and GPS matrix is required. Polysaccharides can be used as stabilizers for metal and metal oxide nanoparticles, which are compatible with the PS matrix because of the similar polysaccharide structures of the PS matrix and the polysaccharide encapsulating the nanoparticles. Some of them have been used as fillers in the PS matrix. The encapsulation of cadmium selenide (CdSe) nanoparticles in the plasticized sago starch matrix was investigated (Bozanic, Djokovic, & Bibic, 2009). ZnO-soluble starch (Ma, Chang, Yu, & Stumborg, 2009), ZnO-carboxymethylcellulose (CMC) (Yu, Yang, Liu, & Ma, 2009) and Sb_2O_3-CMC (Zheng, Chang, Yu, & Ma, 2009) nanoparticles were also incorporated into a PS matrix and resulted in nanocomposites with improved mechanical properties and water resistance. In this work, zirconium hydroxide is fabricated with CMC as the stabilizer in aqueous solution to prepare zirconium hydroxide-CMC (Zr-CMC),

* Corresponding author. Tel.: +86 411 86110419.
E-mail address: maxc1978@sohu.com (X. Ma).

0144-8617/$ – see front matter. Crown Copyright © 2011 Published by Elsevier Ltd. All rights reserved.
doi:10.1016/j.carbpol.2011.06.088

which is used as the filler to enforce the GPS matrix, sourced from *T. kirilowii* (*TK*) starch.

2. Materials and methods

2.1. Materials

T. Kirilowii (*TK*) was purchased from Shandong province, China. For *TK* starch, the amylose content, relative crystallinity and pasting temperature were, respectively 30.3%, 43.1% and 69.7 °C (Ma et al., 2010). Carboxymethyl cellulose sodium (CMC) was analytical grade and provided from Jiang Tian Chemical Technology Co., Ltd. Tianjin, China. Zirconyl chloride ($ZrOCl_2$), glycerol, ammonia and sodium hydroxide were of analytical grade from Tianjin Chemical Reagent Factory, China.

2.2. Isolation of TK starch

The *TK* were washed, cut into small pieces and milled to pass through a 120 mesh sieve. The powders were steeped into 0.02% NaOH solution for 12 h. The supernatant was removed. The starch was washed three times in distilled water. The slurry containing starch was centrifuged in wide-mouthed cups at 3000 rpm for 5 min. The supernatant and upper non-white layer containing the skin and cell wall, were removed. The white layer (starch layer) was suspended in distilled water and centrifuged three times. Finally, *TK* starch was washed with ethanol, and dried overnight at 30 °C.

2.3. Preparation of Zr-CMC

0.75 g CMC was added to 130 mL distilled water. The mixture was heated at 90 °C with constant stirring for the complete dissolution of CMC. The solution was cooled to the room temperature. 40 mL of 8.056 g $ZrOCl_2$ solution was mixed with CMC solution. And 80 mL of NH_3H_2O solution (0.5 mol/L) was added drop-wise with constant stirring at 60 °C. The obtained suspension was aged using ultrasonication for 20 min, aged for another 30 min with constant stirring at 60 °C, separated by centrifugation, washed with distilled water till the pH reached 7, and finally dried at 50 °C.

2.4. The preparation of Zr-CMC/GPS nanocomposites

Zr-CMC was dispersed into the solution of distilled water (100 mL) and glycerol (2 g) using ultrasonication for 10 min. 5 g *TK* starch was added. The Zr-CMC filler loading level (0, 2, 4, 6, 8 or 10 wt%) was based on the *TK* starch. The mixture was heated at 95 °C for 0.5 h for the plasticization of starch with constant stirring. The mixture was cast into a membrane on a dish. The formed solid-like membranes were placed in an air-circulating oven at 50 °C until they were dry (about 6 h). The Zr-CMC/GPS films were preconditioned at 50% RH for at least 48 h prior to the testing.

2.5. Transmission electron microscopy (TEM) and scanning electron microscopy (SEM)

A suspension of Zr-CMC was dropped on a copper grid, then air-dried, and examined using a JEM-1200EX TEM. Starch granules were suspended in the ethanol. The suspension drops were drawn on the glass flake, dried for removing the ethanol, and then vacuum coated with gold for the testing by ESEM, Philips XL-3. The Zr-CMC/GPS films were cooled in liquid nitrogen, and then broken. The fracture surfaces were vacuum coated with gold and examined using a Nanosem 430 scanning electron microscope.

2.6. Fourier transform infrared spectroscopy (FTIR)

FTIR spectra of CMC and Zr-CMC were performed with BIO-RAD FTS3000 IR Spectrum Scanner.

2.7. Thermogravimetric analysis (TGA)

Thermal properties of CMC and Zr-CMC were measured on a ZTY-ZP type thermal analyzer. And Zr-CMC films were analyzed by TG. Sample weight varied from 10 to 15 mg. Samples were heated from room temperature to 600 °C in a nitrogen atmosphere.

2.8. X-ray powder diffraction (XRD)

Zr-CMC was placed in a sample holder for XRD. XRD patterns were tested in the reflection mode in angular range of 10–80° (2θ) at the ambient temperature by a Panalytical X'Pert Pro diffractometer (PANalytical, Holland), operated at 45 kV and 30 mA with the Cu-Kα radiation.

2.9. Ultraviolet–visible (UV–vis)

The UV–vis spectra of Zr-CMC with different concentrations in water were recorded from 250 to 700 nm using a UV–vis spectrophotometer model U-1800, Hitachi Company.

2.10. Mechanical testing

The Testometric AX M350-10KN Materials Testing Machine was operated with a crosshead speed of 50 mm/min for tensile testing (ISO 1184-1983 standard). The data were averaged over 6-8 specimens.

2.11. Water vapor permeability (WVP)

WVP tests were carried out in the methods of Yu, Wang, & Ma (2008) with some modifications. RH 0 was maintained using anhydrous calcium chloride in a cell. The composite films were cut into circles and sealed over the cell with melted paraffin. Each cell was stored in a desiccator containing saturated sodium chloride to provide a constant RH of 75% at 25 °C. WVP was determined by calculating the weight gain of the permeation cell. Changes in the weight of the cell were recorded as a function of time. Slopes were calculated by linear regression (weight change vs. time) and correlation coefficients for all reported data were >0.99. The water vapor transmission rate (WVTR) was defined as the slope (g/s) divided by the transfer area (m^2). After the permeation tests, film thickness was measured and WVP ($g\,Pa^{-1}\,s^{-1}\,m^{-1}$) was calculated as:

$$\mathrm{WVP} = \frac{\mathrm{WVTR}}{P(R_1 - R_2)}x \quad (1)$$

where P is the saturation vapor pressure of water (Pa) at the test temperature (25 °C), R_1 is the RH in the desiccator, R_2, is the RH in the permeation cell and x is the film thickness (m). Under these conditions, the driving force $[P(R_1 - R_2)]$ is 1753.55 Pa.

3. Results and discussion

3.1. Characterization of Zr-CMC

As shown in Fig. 1a, zirconium hydroxide particles were in size of 20–50 nm. And the particles were covered with CMC. In Fig. 1b, the central black spot and light colored edge represented zirconium hydroxide nanoparticles and CMC, respectively. Since polysaccharides could form complexes with metal ions due to their high number of coordinating functional groups (hydroxyl and glucoside

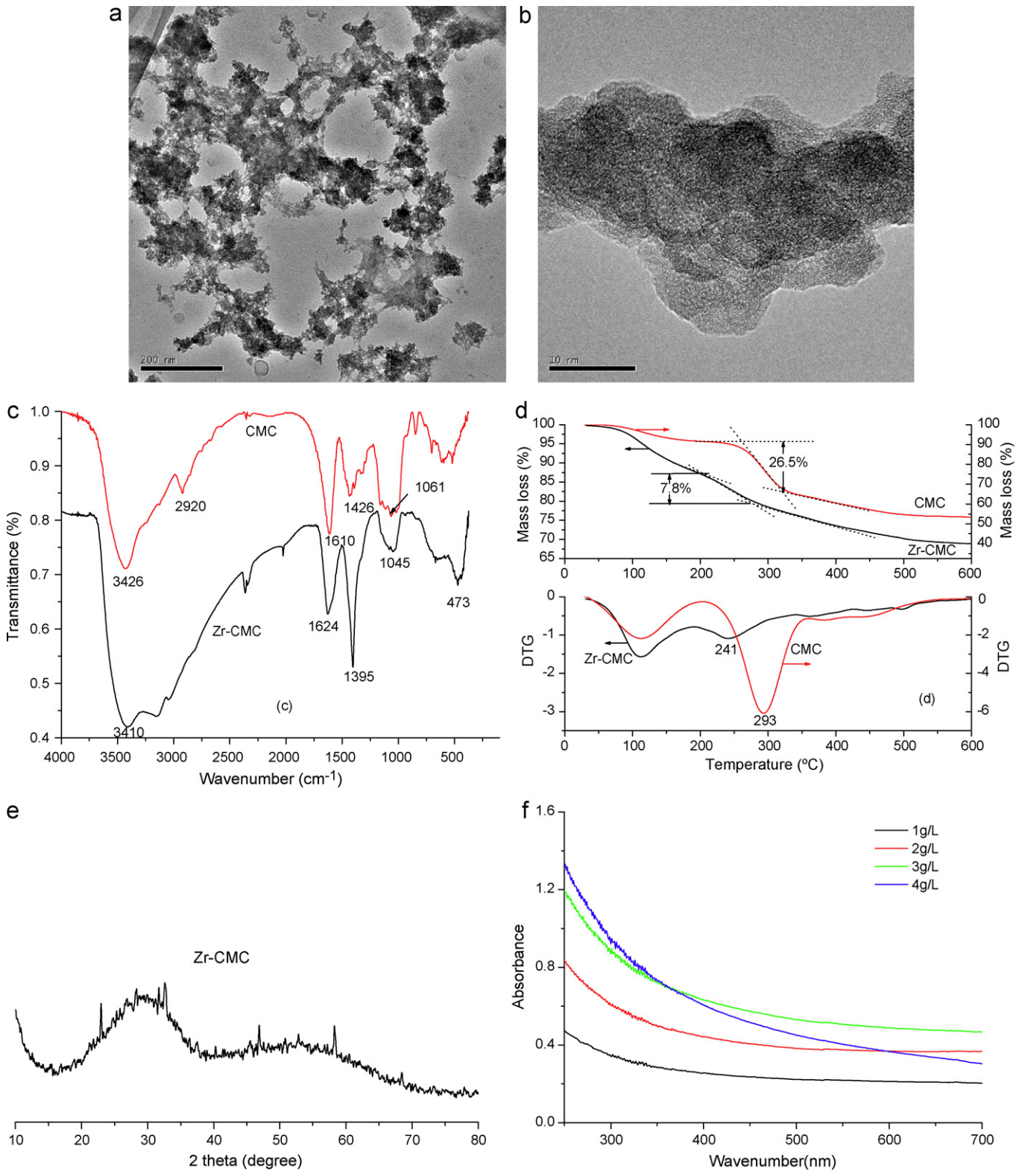

Fig. 1. (a) and (b) TEM of Zr-CMC; (c) FTIR of spectra of CMC and Zr-CMC; (d) the thermogravimetric (TG) and derivative thermogravimetric (DTG) curves of CMC and Zr-CMC (d); (e) XRD patterns of Zr-CMC (f) UV–visible absorption of Zr-CMC with the different concentrations in water.

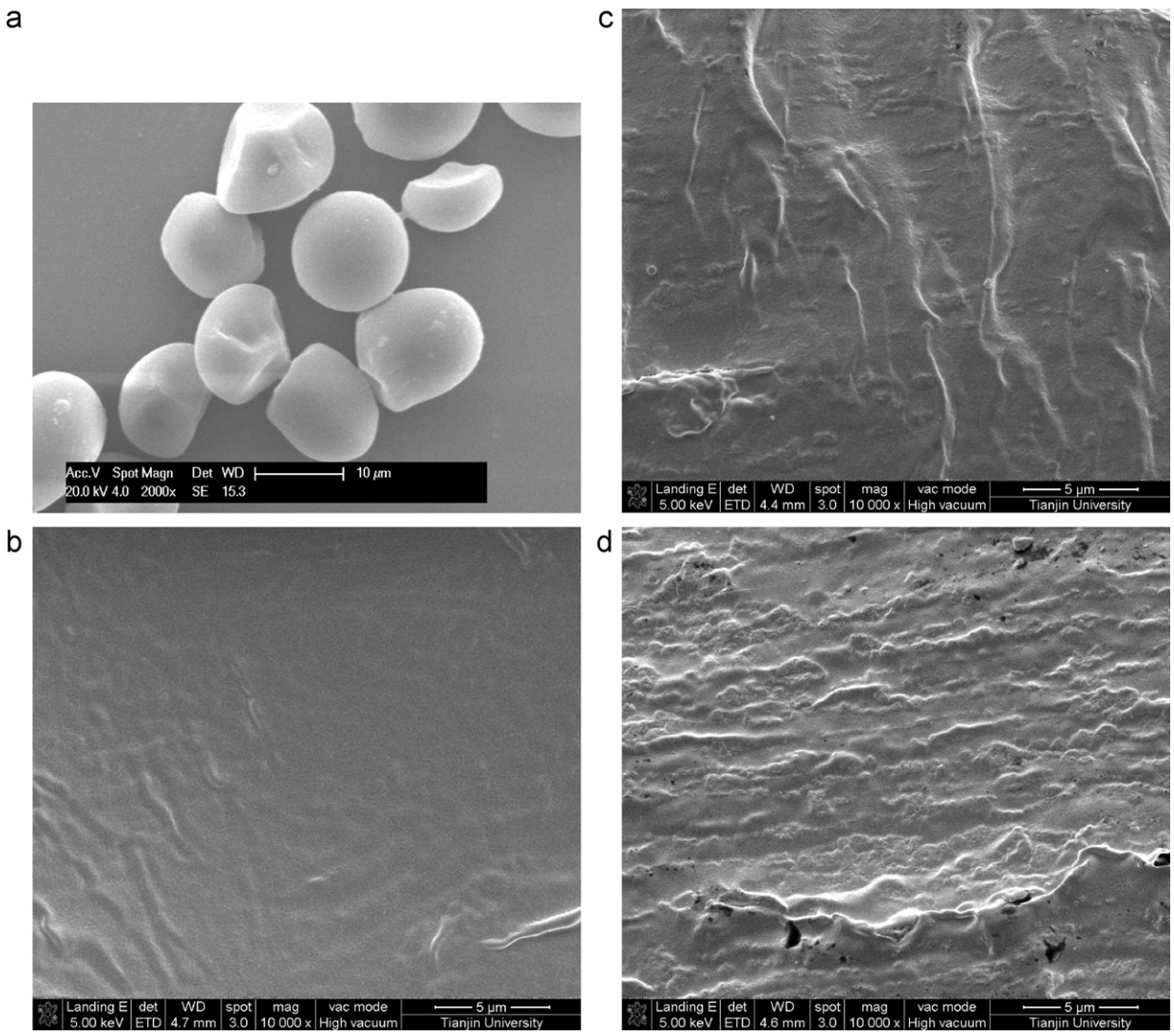

Fig. 2. SEM micrograph of *TK* starch (a) and the fragile fractured surface of the Zr-CMC/GPS films with different Zr-CMC contents, (b) 0 wt%, (c) 2 wt% and (d) 8 wt%.

groups) (Taubert & Wegner, 2002), CMC could improve the stability of zirconium hydroxide in water and prevent further aggregation of zirconium hydroxide, resulting in the formation of zirconium hydroxide nanoparticles encapsulated by CMC.

The infrared spectra for the zirconium hydroxide-CMC and CMC are illustrated in Fig. 1c. As shown in the FTIR spectra of CMC, a broad band centered at 3426 cm^{-1} was ascribed to a wide distribution of hydrogen-bonded hydroxyl groups. And the peak at 2920 cm^{-1} was related to C–H stretching of methylene on polysaccharide rings (Yu et al., 2009). Two peaks located at 1420 and 1610 cm^{-1} corresponding to the symmetrical and asymmetrical stretching vibrations of the carboxylate groups (Rosca, Popa, & Lisa, 2005). And the absorption bands of the –C–O– stretching on polysaccharide skeleton were between 1000 and 1200 cm^{-1}. In the FTIR spectra of Zr-CMC, the broad bands at 3000–3500 cm^{-1} resulted from the OH groups of both CMC and the zirconium hydroxide. The band at 1395 cm^{-1} was attributed to bidentate carbonates formed by the "side-on" coordination of atmospheric constituent CO_2 on coordinatively unsaturated O^{-2}–Zr^{4+} pairs. And the band at 473 cm^{-1} was indicative of Zr–O bond vibration (Guo & Chen, 2004). The band, ascribed to –C–O– stretching on polysaccharide skeleton, shifted to the lower wavenumbers. It confirmed that the interaction existed between zirconium hydroxide and C–O groups of CMC (Pawlak & Mucha, 2003). In addition, the peak of the C–H stretching at 2920 cm^{-1} and the bands of OH groups could be overlapped in the FTIR spectra of Zr-CMC.

The TG and derivative thermogravimetric (DTG) curves of Zr-CMC and CMC are shown in Fig. 1d. The decomposition temperature appeared at the maximum rate of mass loss in TG curves, i.e. the peak temperature shown in DTG curves. The mass losses were determined in method of tangential lines, as described in Fig. 1d. The Zr-CMC showed two obvious decompositions. The first mass loss of about 10 wt% was mainly ascribed to water loss before 150 °C, which could be composed of two parts. One part was sourced from the free water of CMC, which could be confirmed from the TG and DTG curves of CMC. The other part was the coordinated water in presented zirconium hydroxide (Guo & Chen, 2004). The second mass loss of about 7.8 wt% was the degradation of CMC components in Zr-CMC at the range of 200–350 °C, while the mass loss of CMC was about 26.5 wt%. It was assumed that the percentages of mass loss of CMC were constant when zirconium hydroxide was incorporated with CMC. The content of CMC (about 29.4 wt%) in Zr-CMC could be calculated by matching 7.8–26.5 wt%. And CMC exhibited the better thermal stability than CMC in Zr-CMC. It could be ascribed to the degradation of CMC in the preparation processing of Zr-CMC.

XRD pattern of Zr-CMC is shown in Fig. 1e. Although there are no sharp diffraction peaks corresponding to a crystalline phase, there

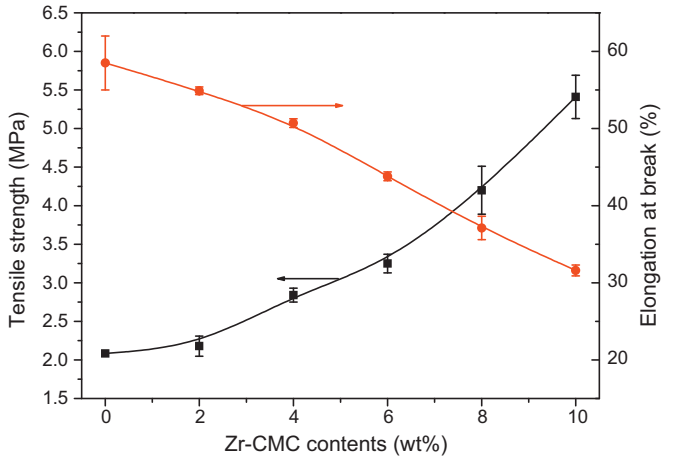

Fig. 3. The effect of Zr-CMC contents on tensile strength and elongation at break of the Zr-CMC/GPS films.

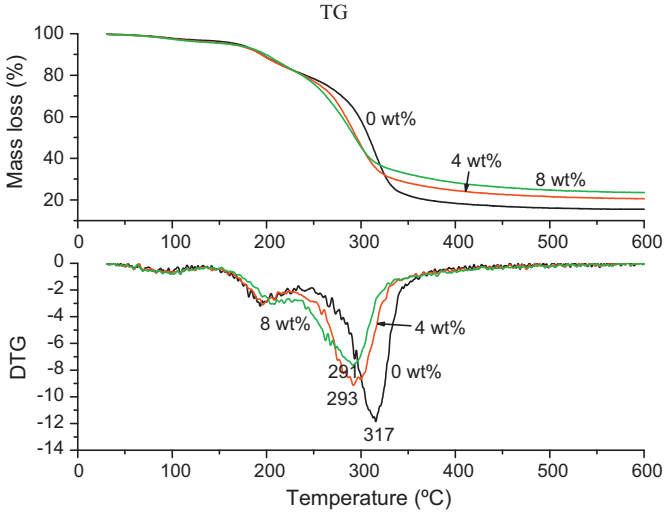

Fig. 4. The effect of Zr-CMC contents on the thermal stability of the Zr-CMC/GPS films.

are a number of broad peaks. The diffraction patterns of amorphous zirconium hydroxide generally contain some very broad peaks (Southon, Bartlett, Woolfrey, & Ben-Nissan, 2002). The similar diffraction pattern has been observed for amorphous zirconium hydroxide (Chitrakar et al., 2006).

Fig. 1f exhibited the UV–vis absorbance of Zr-CMC with different concentrations in water. In the 250–800 nm regions, the basically linear relationship between the absorbance and Zr-CMC concentrations (at below 3 g/L) indicated that Zr-CMC were uniformly dispersed in water. CMC components could improve the hydrophilicity of Zr-CMC, which facilitated the dispersion of Zr-CMC in water. However, more concentration (4 g/L) resulted in the aggregations of Zr-CMC in water.

3.2. Scanning electron microscopy (SEM)

Native *TK* starch is in the size of about 10(m in Fig. 2a. As shown in Fig. 2b, no residual granular structure of starch was observed in the continuous GPS phase. At the high temperature, water and glycerol were known to physically break up the granules of starch and disrupt intermolecular and intramolecular hydrogen bonds and make the native starch plastic (Xie et al., 2011). Similar to the corn and potato starch, which were often used for plastic starch materials, *TK* starch also was plasticized as the continuous matrix of the fillers.

The distribution of Zr-CMC in the matrix of GPS was shown in Fig. 2 (c and d). Zr-CMC agglomeration in size of a few hundred nanometers could be evenly dispersed in GPS matrix, when the content of Zr-CMC was 2 wt%. More agglomeration of Zr-CMC in lager size of 1–2 (m appeared in the Zr-CMC/GPS composites with higher Zr-CMC content (8 wt%). In addition, the surface of Zr-CMC was obviously covered by GPS, and no gap between the filler and the matrix was observed. These could be attributed to the strong interaction between CMC and starch-based matrix due to their similar polysaccharide structure.

3.3. Mechanical properties of Zr-CMC/GPS composites

Fig. 3 exhibited the dependence of mechanical properties on Zr-CMC contents. As the filler of GPS matrix, Zr-CMC had an obvious reinforcing effect. With the increasing of Zr-CMC contents, tensile strength of Zr-CMC/GPS composites increased much, but the elongation at break decreased. When Zr-CMC contents varied from 0 to 10 wt%, tensile strength increased from 2.08 MPa to 5.41 MPa, while the elongation at break decreased from 58.5% to 31.6%. Generally, the well-dispersed fillers could constrain the surrounding polymers, decrease the mobility of matrix chains, and further result in the higher tensile strength and lower elongation at break. The good dispersion of Zr-CMC in GPS matrix was related to the good interfacial interaction between the Zr-CMC fillers and GPS matrix, because *TK* starch and CMC possessed the similar polysaccharide structure.

3.4. Thermal stability of Zr-CMC/GPS composites

TG and DTG curves of Zr-CMC/GPS composites were shown in Fig. 4. The mass loss of GPS before the onset temperature was related to the volatilization of both water and glycerol plasticizer (Ma, Chang, Yu, et al., 2009). There was little difference in mass loss among GPS and Zr-CMC/GPS composites at onset temperature, mainly because of the similar water and glycerol contents. With the increasing of Zr-CMC contents, the degradation of GPS and Zr-CMC/GPS composites, respectively took place at 317, 293 and 291 °C. The addition of Zr-CMC resulted in the decreasing of thermal stability. It could be ascribed to the poor thermal stability of CMC in ZR-CMC, the decomposition temperature of which was 241 °C, as shown in Fig. 1d. The decomposition of CMC components could accelerate the decomposition of the matrix. GPS/CMC composites had similar results (Ma, Chang, & Yu, 2008). It was also noted that the residues at the high temperature (500 °C) were improved with increased loading of Zr-CMC, because the decomposition of zirconium hydroxide components had not occurred at 500 °C.

3.5. WVP of Zr-CMC/GPS composites

Water vapor permeability (WVP) is often used to study the moisture transport through the film. Fig. 5 exhibited the moisture transport through the Zr-CMC/GPS films with different Zr-CMC contents. Water vapor easily went through the GPS film with the highest WVP values of 5.69×10^{-9} g^{-1} s^{-1} Pa^{-1}. With the increasing of Zr-CMC contents, WVP values decreased obviously. The addition of Zr-CMC probably introduced a tortuous path for water molecule to pass through (Kristo & Biliaderis, 2007). At the low Zr-CMC loading contents (below 6 wt%), Zr-CMC could disperse well in the matrix. There were few paths for water molecule to pass through. At the high contents of Zr-CMC, the aggregation of Zr-CMC could counteract the addition of Zr-CMC. Therefore, the WVP decreased only slightly from 4.85×10^{-9} g^{1} s^{-1} Pa^{-1} at 6 wt% to

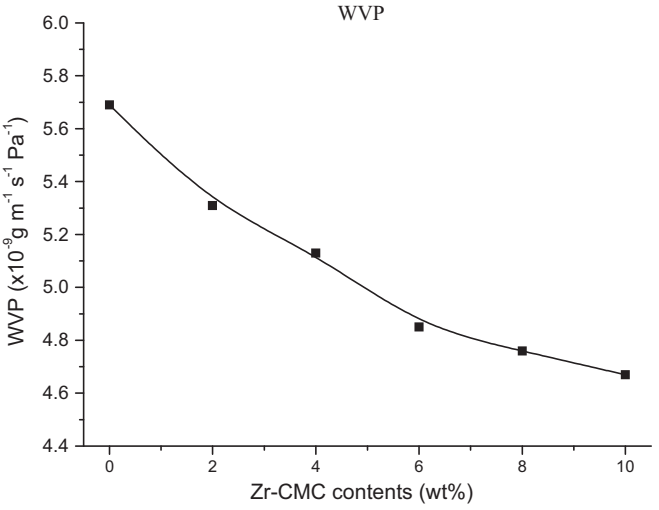

Fig. 5. The effect of Zr-CMC contents on water vapor permeability of the Zr-CMC/GPS films.

4.67×10^{-9} g/s Pa^{-1} at 10 wt%. In general, the composites exhibited better moisture barrier in comparison with pure GPS film.

4. Conclusions

Zr-CMC nanoparticles were prepared with CMC as the template, in which amorphous zirconium hydroxide particles in the size of about 20–50 nm were encapsulated by CMC. *TK* starch was firstly plasticized by glycerol as the matrix of Zr-CMC fillers. CMC played a very important role on the preparation of both Zr-CMC and Zr-CMC/GPS composites. The good interaction existed between the filler and GPS matrix, due to CMC encapsulating zirconium hydroxide nanoparticles. This interaction improved the dispersion of the fillers in GPS matrix; thereby enhanced tensile strength and water vapor resistance with the increasing of Zr-CMC contents. However, the poor thermal stability of CMC components in Zr-CMC could decrease the thermal stability of the nanocomposites. In addition, *TK* starch was confirmed to use for plasticized materials similar to traditional crop starches.

References

Averous, L., Moro, L., Dole, P., & Fringant, C. (2000). Properties of thermoplastic blends: starch–polycaprolactone. *Polymer*, *41*, 4157–4167.

Bozanic, D. K., Djokovic, V., & Bibic, N. (2009). Biopolymer-protected CdSe nanoparticles. *Carbohydrate Research*, *344*, 2383–2387.

Chitrakar, R., Tezuka, S., Sonoda, A., Sakane, K., Ooi, K., & Hirotsu, T. (2006). Selective adsorption of phosphate from seawater and wastewater by amorphous zirconium hydroxide. *Journal of Colloid and Interface*, *297*, 426–433.

Dias, A. B., Müller, C. M. O., Larotonda, F. D. S., & Laurindo, J. B. (2010). Biodegradable films based on rice starch and rice flour. *Journal of Cereal Science*, *51*, 213–219.

Forssell, P. M., Hulleman, S. H. D., Myllārinen, P. J., Moates, G. K., & Parker, R. (1999). Ageing of rubbery thermoplastic barley and oat starches. *Carbohydrate Polymers*, *39*, 43–51.

Guo, G. Y., & Chen, Y. L. (2004). New zirconium hydroxide. *Journal of Materials Science*, *39*, 4039–4043.

Kristo, E., & Biliaderis, C. G. (2007). Physical properties of starch nanocrystal-reinforced pullulan films. *Carbohydrate Polymers*, *68*, 146–158.

Ma, X. F., Chang, P. R., Yang, J. W., & Yu, J. G. (2009). Preparation and properties of glycerol plasticized-pea starch/zinc oxide–starch bionanocomposites. *Carbohydrate Polymers*, *75*, 472–478.

Ma, X. F., Chang, P. R., & Yu, J. G. (2008). Properties of biodegradable thermoplastic pea starch/carboxymethyl cellulose and pea starch/microcrystalline cellulose composites. *Carbohydrate Polymers*, *72*, 369–375.

Ma, X. F., Chang, P. R., Yu, J. G., & Stumborg, M. (2009). Properties of biodegradable citric acid-modified granular starch/thermoplastic pea starch composites. *Carbohydrate Polymers*, *75*, 1–8.

Ma, X. C., Chang, P. R., Zheng, P. W., Yu, J. G., & Ma, X. F. (2010). Characterization of new starches separated from several traditional Chinese medicines. *Carbohydrate Polymers*, *82*, 148–152.

Mali, S., Grossmann, M. V. E., García, M. A., Martino, M. N., & Zaritzky, N. E. (2006). Effects of controlled storage on thermal, mechanical and barrier properties of plasticized films from different starch sources. *Journal of Food Engineering*, *75*, 453–460.

Mondragon, M., Mancilla, J. E., & Rodriguez-Gonzalez, F. J. (2008). Nanocomposites from plasticized high-amylopectin, normal and high-amylose maize starches. *Polymer Engineering and Science*, *48*, 1261–1267.

Pawlak, A., & Mucha, M. (2003). Thermogravimetric and FTIR studies of chitosan blends. *Thermochimica Acta*, *396*, 153–166.

Rosca, C., Popa, M. I., & Lisa, G. (2005). Interaction of chitosan with natural or synthetic anionic polyelectrolytes. 1. The chitosan–carboxymethylcellulose complex. *Carbohydrate Polymers*, *62*, 35–41.

Smits, A. L. M., Kruiskamp, P. H., van Soest, J. J. G., & Vliegenthart, J. F. G. (2003). Interaction between dry starch and plasticisers glycerol or ethylene glycol, measured by differential scanning calorimetry and solid state NMR spectroscopy. *Carbohydrate Polymers*, *53*, 409–416.

Southon, P. D., Bartlett, J. R., Woolfrey, J. L., & Ben-Nissan, B. (2002). Formation and characterization of an aqueous zirconium hydroxide colloid. *Chemistry of Materials*, *14*, 4313–4319.

Taubert, A., & Wegner, G. (2002). Formation of uniform and monodisperse zincite crystals in the presence of soluble starch. *Journal of Materials Chemistry*, *12*, 805–807.

Wang, S. J., Yu, J. L., Gao, W. Y., Pang, J. P., Yu, J. G., & Xiao, P. G. (2007). Characterization of starch isolated from Fritillaria traditional Chinese medicine (TCM). *Journal of Food Engineering*, *80*, 727–734.

Wang, S. J., Yu, J. L., Zhu, Q. H., Yu, J. G., & Jin, F. M. (2009). Granular structure and allomorph position in C-type Chinese yam starch granule revealed by SEM, C-13 CP/MAS NMR and XRD. *Food Hydrocolloids*, *23*, 426–433.

Xie, Y. F., Chang, P. R., Wang, S. J., Yu, J. G., & Ma, X. F. (2011). Preparation and properties of halloysite nanotubes/plasticized Dioscorea opposita Thunb. starch composites. *Carbohydrate Polymers*, *83*, 186–191.

Yu, J. G., Wang, N., & Ma, X. F. (2008). Fabrication and characterization of poly(lactic acid)/acetyl tributyl citrate/carbon black as conductive polymer composites. *Biomacromolecules*, *9*, 1050–1057.

Yu, J. G., Yang, J. W., Liu, B. X., & Ma, X. F. (2009). Preparation and characterization of glycerol plasticized-pea starch/ZnO-carboxymethylcellulose sodium nanocomposites. *Bioresource Technology*, *100*, 2832–2841.

Zheng, P. W., Chang, P. R., Yu, J. G., & Ma, X. F. (2009). Preparation of Sb_2O_3–carboxymethyl cellulose sodium nanoparticles and their reinforcing action on plasticized starch. *Starch-Starke*, *61*, 665–668.

Zhou, H. Y., Wang, J. H., Zhao, H. J., Fang, X. S., & Sun, Y. S. (2010). Characterization of starches isolated from different Chinese Baizhi (*Angelica dahurica*) cultivars. *Starch-Starke*, *62*, 198–204.